International Journal of Electrochemical Science 20 (2025) 100909

Contents lists available at ScienceDirect

International Journal of Electrochemical Science

journal homepage: www.editorialmanager.com/ijoes

Effect of tin alloying on the corrosion behavior and discharge performance of aluminum anodes for aluminum-air batteries

Bilgehan Çetinöz Öksüz [a,*], Metehan Erdoğan [b], İshak Karakaya [a]

[a] Metallurgical and Materials Engineering, Middle East Technical University, Ankara, Turkey
[b] Metallurgical and Materials Engineering, Ankara Yıldırım Beyazıt University, Ankara, Turkey

ARTICLE INFO

Keywords:
Aluminum air battery
Metal air batteries
Aluminum alloying
Corrosion

ABSTRACT

Aluminum-air batteries (AAB) are alternative to common commercial batteries like lithium-ion batteries due to their high theoretical energy density, low cost, and environmental friendliness. However, the formation of a protective oxide layer and side corrosion reactions on aluminum anodes limit the efficiency and decreases energy density. Effect of tin (Sn) alloying on the corrosion rate and discharge behavior of aluminum alloys for AABs in an alkaline solution was investigated in this study. Al-0.5Mg-0.05Ga-0.05In base alloy having three different Sn compositions were used during immersion and electrochemical tests performed in 4 M NaOH solution. The results show that addition of Sn significantly affects the self-corrosion rate and discharge performance of alloy. The alloy containing 0.1 wt% Sn exhibited the lowest corrosion rate and the highest energy density, highlighting the optimal Sn concentration for enhanced AAB performance. Microstructural analysis using SEM (Scanning Electron Microscope) and EDS (Energy Dispersive Spectroscopy) confirmed the presence of Sn-rich precipitates, which influence the electrochemical behavior of the alloys.

1. Introduction

Conventional energy sources, which are based on fossils, are facing challenges such as resource depletion, risks to human health and other concerns. Additionally, extracting fossil fuels from the earth and burning them to meet various human energy needs raises numerous concerns, including climate change, pollution, and long-term environmental damage [1]. Electrochemical energy storage devices are crucial for the future energy grid, helping to stabilize the variable energy production and supply from renewable sources. Achieving this expansion requires the development of efficient, cost-effective, and environmentally friendly battery systems. At present, the most commonly used batteries are lead-acid, nickel-cadmium, and lithium-ion, which are employed in portable devices and electric vehicles (EVs). While there have been significant advancements in lithium-ion technology, their practical energy densities still fall short for providing the extended range required for EVs. Additionally, these batteries are costly and may pose safety concerns. Lithium-ion batteries (LIBs) are the primary power source for EVs, but challenges related to lithium supply and disposal are already emerging [2]. Among the various promising options, metal-air batteries, which use oxygen or air as a feedstock, have garnered renewed interest. These batteries consist of a metal anode, an air-breathing cathode, and an appropriate electrolyte. The metal anode can be alkali metals (like Li, Na, and K), alkaline earth metals (such as Mg), or first-row transition metals (such as Fe and Zn) with favorable electrochemical properties. Metal-air batteries incorporate design elements from both traditional batteries and fuel cells and offer a theoretical energy density that is approximately 3–30 times greater than that of lithium-ion batteries [3]. Primary and secondary metal–air batteries, including zinc (Zn)–, aluminum (Al)–, lithium (Li)–, iron (Fe)–, and magnesium (Mg)–air batteries, have received considerable attention. Aluminum is lightweight, inexpensive, and abundant [4], and Al-air batteries (AAB) systems are predicted to be safer than lithium-based designs [5]. Even magnesium-air battery has higher theoretical energy density (6800 W h kg^{-1}) [6], magnesium has a more negative standard electrode potential (-2.37 V vs. SHE) compared to aluminum (-1.66 V vs. SHE), making it more prone to oxidation and corrosion [6,7]. Aluminum has higher corrosion resistance compare to magnesium. The oxidation product of magnesium ($Mg(OH)_2$) is not strongly adherent and does not provide an effective protective barrier, leading to continued exposure to corrosive environments [8]. Aluminum and aluminum-air batteries are generally safer than magnesium-air batteries due to lower reactivity,

* Corresponding author.
E-mail address: e219390@metu.edu.tr (B.Ç. Öksüz).

https://doi.org/10.1016/j.ijoes.2024.100909
Received 22 October 2024; Received in revised form 2 December 2024; Accepted 4 December 2024
Available online 5 December 2024
1452-3981/© 2024 The Author(s). Published by Elsevier B.V. on behalf of ESG. This is an open access article under the CC BY license (http://creativecommons.org/licenses/by/4.0/).

Table 1
The elemental composition of the aluminum alloys (wt%).

Specimens	Mg	Ga	In	Sn	Al
Alloy 1	0.521	0.048	0.051	-	Balance
Alloy 2	0.517	0.051	0.051	0.091	Balance
Alloy 3	0.492	0.048	0.052	0.223	Balance
Alloy 4	0.523	0.050	0.050	0.407	Balance

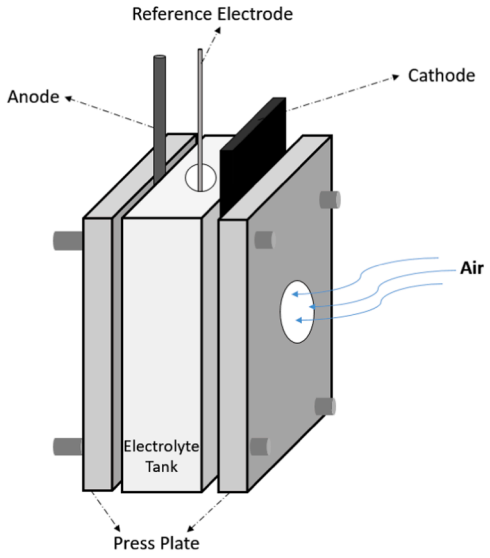

Fig. 1. Schematic diagram of single cell of Al-air battery.

better corrosion resistance, and lower risk of uncontrolled hydrogen generation of aluminum.

Currently, the Al-air battery is less popular than the Zn-air battery. The primary issue is that the aluminum (Al) anode has some undesirable properties, notably the formation of a protective oxide film on its surface when exposed to air and aqueous solutions. This oxide film shifts the corrosion potential of the Al electrode positively by nearly −0.8 V, significantly slowing down the active dissolution of Al and leading to a substantial loss of available energy. The other reason which makes aluminum less attractive anode is side corrosion reaction. As a result, Al is not considered an ideal anode material for energy applications [9–11]. In literature, there are several studies which suppressed corrosion side reaction in aluminum air battery (AAB) using corrosion inhibitors [12–14] and by alloying aluminum [15–21]. Corrosion inhibitors suppress the corrosion reaction and help maintaining the efficiency of the aluminum-air battery by minimizing side reactions that consume aluminum without generating electricity. But this is the only effect of using a corrosion inhibitor in an aluminum-air battery. However, desired properties can be obtained by alloying aluminum with Mg, Ga, Sn, In, Zn, Mn etc. Both surface activation can be increased and corrosion behavior can be improved by alloying aluminum. More active surface provides higher cell voltage and lower corrosion rate increases the cell efficiency [12–18]. Addition of Mg in aluminum alloy was studied before and the results show addition of Mg likely enhances aluminum resistance to impurities by forming compounds with elements such as silicon, which inhibits these elements from serving as sites for hydrogen evolution. Additionally, magnesium may shift the potential of the aluminum anode in a negative direction and reduce self-corrosion. The passive film is further activated through Mg^{2+} doping, which improves the rate of ionic migration [22,23]. Gao et al. investigated four magnesium concentrations: 0.5 %, 2 %, 4 %, and 8 %. It was observed that when the magnesium content exceeds 3 %, Al_3Mg_2 tends to accumulate along the grain boundaries. Optimized concentration of Mg in Al anode was selected to be 0.5 % [21]. Gallium on the alloy surface weakened the Al_2O_3 oxide layer by causing it to crack and get thinner, which facilitated continuous aluminum diffusion and dissolution. With a low melting point of 29.8°C, gallium is highly soluble in aluminum, up to 21 wt%. The presence of 50–1000 ppm Ga in homogenized AlGa binary alloys did not result in anodic activation, as gallium remained stable in solid solution. The Ga elements are consistently and uniformly dissolved within the Al matrix, displaying a homogeneous distribution. This uniformity arises from high solid solubility of Ga in Al [24]. According to a study by McDonald et al., the lowest corrosion current (i_{corr}) was achieved with 0.05 % Ga. Similarly, the lowest hydrogen evolution was also observed at 0.05 % Ga [25]. Addition of indium to aluminum alloy increases activity by disrupted oxide layer. Addition of indium also decreases the hydrogen evolution rate because of high hydrogen evolution overpotential (HER onset potential vs SCE −0.47 V for Aluminum, −0.80 V for Indium). $In(OH)_3$ is formed in alkaline solution and this discharge product form new passivation layer on aluminum [17–25]. Tin is another common alloying metal for aluminum air battery due to its high hydrogen overpotential. The literature includes some examples that highlight the effect of tin (Sn) on aluminum-air batteries [26–28]. X. Xu et al. examined 4 different alloy compositions to investigate the effect on Al-Mg based alloys. They found that anode efficiency increases with the tin content up to 0.5 wt%, but when the tin content exceeds this amount, anode efficiency decreases. X. Xu et al. attributed these results to the tin-rich phases which act as catodic sites [26]. Elrouby et al. compared pure aluminum with Al-Sn and Al-Zn alloy anodes and they showed that both discharge voltage and time increase when pure aluminum was alloyed with Sn and Zn [27]. The effect of Sn in Al-0.2Mg-0.02In-0.04Ga-0.02Bi base alloy was investigated by Sui et al. Results showed that the alloy anode achieves optimal overall performance when the Sn content was 0.03 % [28].

Other than the above limited information, detailed study of the effect of tin on the anode performance of Al-Mg-Ga-based alloy in AAB is not available. The effect of Sn content was examined using an Al-0.5Mg-0.05Ga-0.05In base alloy for aluminum-air batteries in this study. Three different Sn compositions were tested in 4 M NaOH electrolyte to assess the electrochemical performance of the alloyed aluminum. An immersion test was conducted to evaluate the impact of Sn content on the corrosion rate, while discharge tests were performed to compare the discharge efficiency of various aluminum alloy compositions. Microstructural analyses of the cast alloys, along with electrochemical impedance spectroscopy (EIS), were performed to better understand the mechanism by which Sn influences the Al-0.5Mg-0.05Ga-0.05In base alloy.

2. Experimental

2.1. Material preparation

Commercially pure (series 1000) aluminum ((> 99.5 wt% balanced with Fe (0.19 wt%) and Si (0.11 wt%)), magnesium (> 99 wt%), tin (> 99.99 wt%), indium (> 99.99 wt%), and gallium (> 99.99 wt%) were used as raw materials to cast Al-0.5Mg-0.05Ga-0.05In (wt%) (Alloy 1), Al-0.5Mg-0.05Ga-0.05In-0.1Sn (wt%) (Alloy 2), Al-0.5Mg-0.05Ga-0.05In-0.2Sn (wt%) (Alloy 3) and Al-0.5Mg-0.05Ga-0.05In-0.4Sn (wt %) (Alloy 4). The casting process was carried out using a vacuum induction furnace (Indutherm MC 20 V) at 770 ºC under argon atmosphere. The molten alloy was poured into a preheated copper dye under argon atmosphere at 3 bars.

Aluminum composition of the alloys was analyzed while the amount of In was estimated using ICP-OES (Inductively Coupled Plasma–Optical Emission Spectroscopy) and the amounts of Mg, Ga, Mn and Sn were analyzed using Arc/Spark-OES. Table 1 gives the results of elemental analysis of cast aluminum alloys. Also, X-Ray diffraction analysis (XRD) was conducted to reveal alloying effect on crystal lattice.

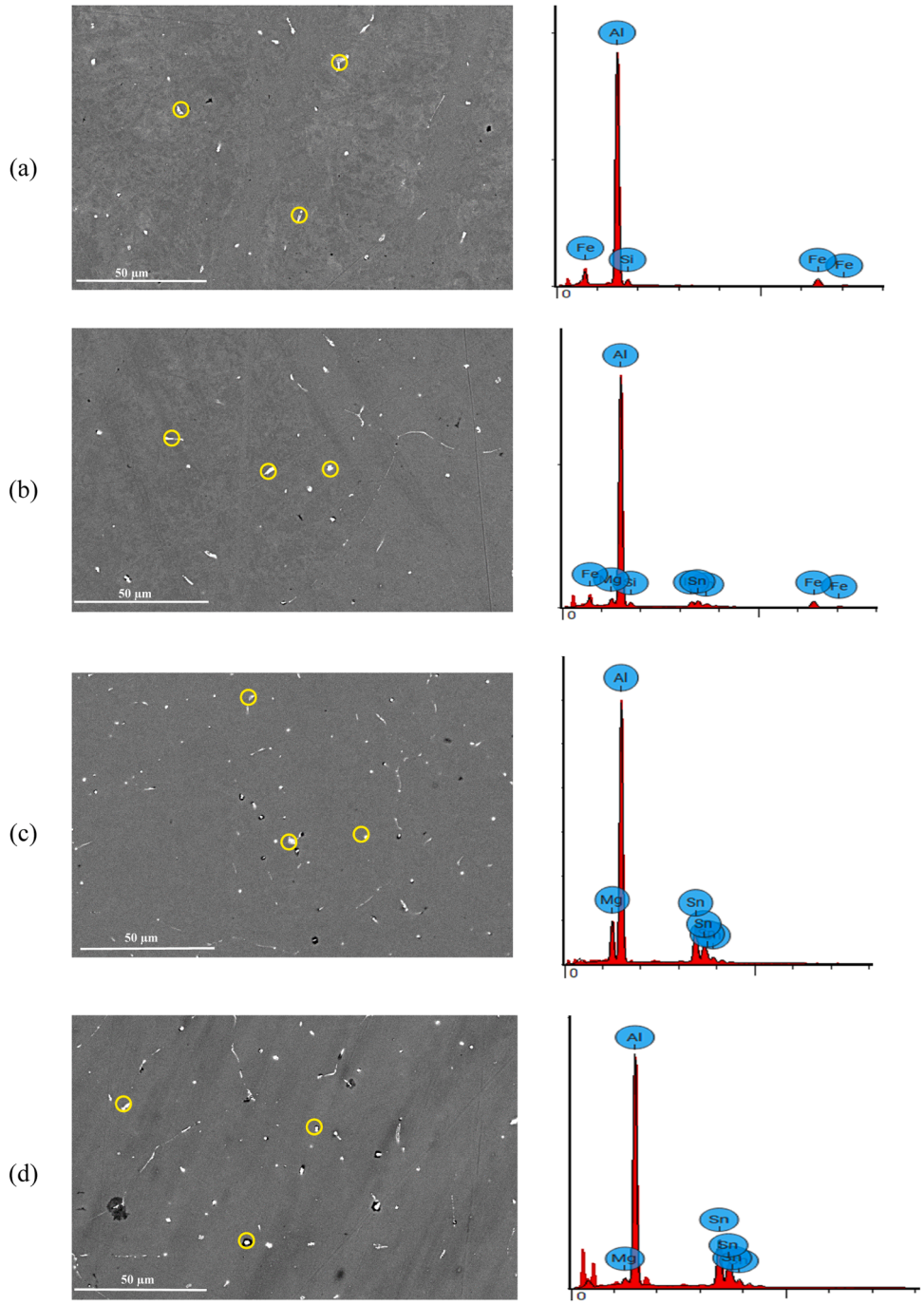

Fig. 2. SEM images (back scatter) and EDS Analysis of (a) Alloy 1, (b) Alloy 2, (c) Alloy 3 and (d) Alloy 4.

2.2. Self-corrosion

Each specimen was weighed using a precision scale before being immersed into 4 M NaOH. After exposure to 4 M NaOH for 1 hour, the specimens were weighed again. The difference between the two measurements provided the experimental weight loss. The corrosion rate was calculated using Eq. 1.

$$Corrosion\ Rate(mmpy) = \frac{8.76x10^4 x \text{Weigth loss}_{experimental}}{Axtx\varrho} \quad (1)$$

where A is surface area (cm^2) which is exposed to solution, t is immersion time (hours) and ϱ is density (g/cm^3) of aluminum alloys which is assumed to be 2.71 g/cm^3.

2.3. Electrochemical Measurements

Electrochemical measurements (discharge test and electrochemical impedance spectroscopy (EIS)) were conducted using a three-electrode system at room temperature by a Gamry Reference 3000 Potentiostat/Galvanostat/ZRA. A Saturated Calomel Electrode (SCE) served as the reference [4]. M NaOH was used as electrolyte. Cylindrical specimens (Ø 12 mm×20 mm) were prepared and mounted in epoxy resin, leaving the circular base exposed. This confined a circular exposed area (1.7 cm^2). All specimens were sanded and polished prior to electrochemical measurements.

The Gamry MultiPort Corrosion Cell Kit was used to maintain a fixed distance between the electrodes during the EIS test. A graphite rod was employed as the counter electrode. The EIS test was performed over a

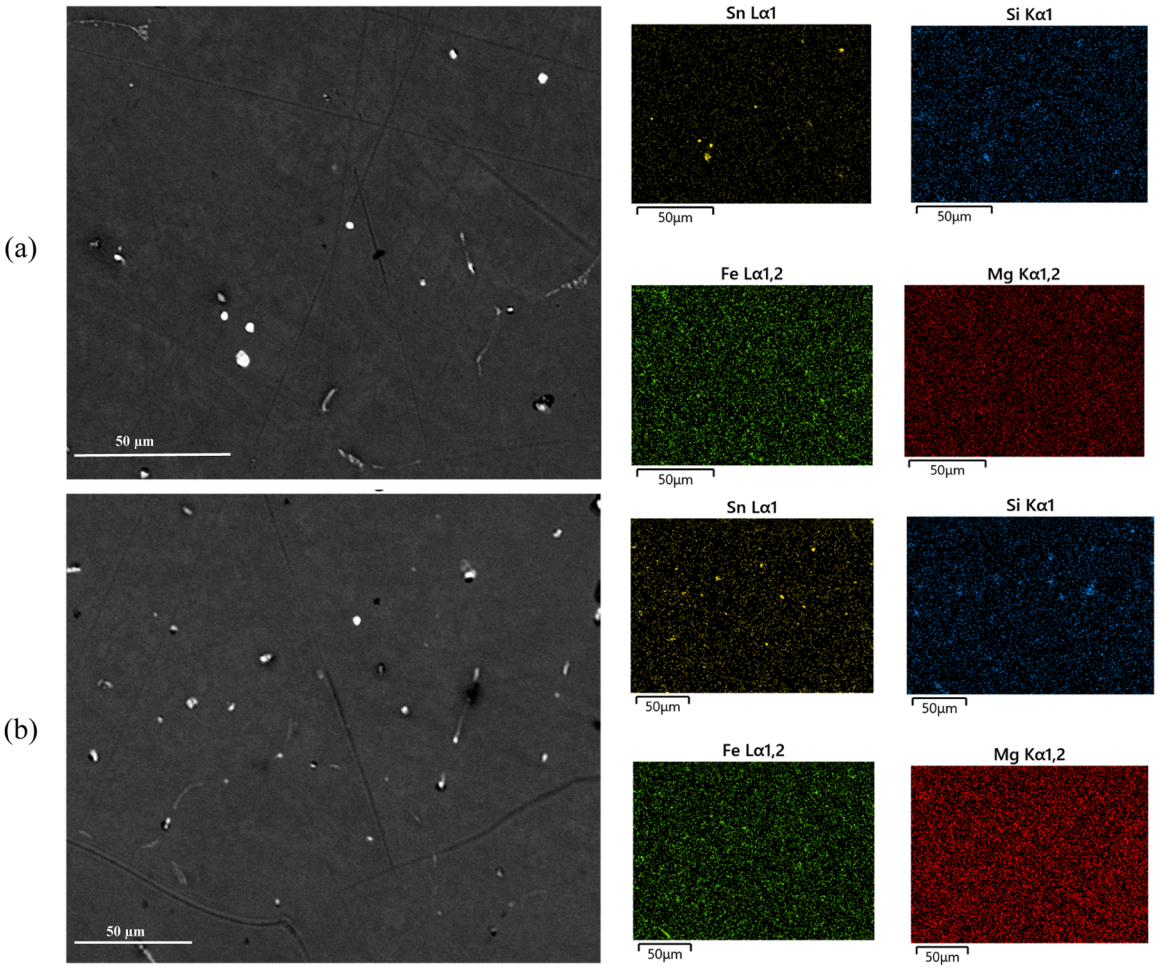

Fig. 3. Elemental mappings for (a) Al-0.5Mg-0.05Ga-0.01In-0.1Sn (Alloy 2) and (b) Al-0.5Mg-0.05Ga-0.01In-0.4Sn (Alloy 4).

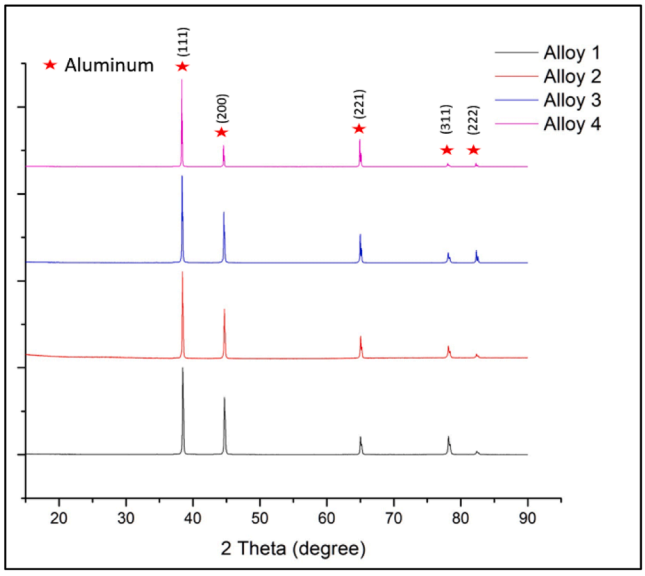

Fig. 4. XRD Patterns of Alloy 1, Alloy 2, Alloy 3 and Alloy 4.

frequency range of 1000 kHz to 0.1 Hz at open circuit voltage (OCV).

Full cell test setup was designed and it is shown in Fig. 1. Commercial carbon (High Performance Alkaline Air Diffusion Electrode (ADE) with Non-Precious Metal Catalyst from Fuel Cell Store) was used as cathode.

Table 2
Immersion test results of aluminum alloys in 4 M NaOH.

Alloy	Weight Loss (mg)	Corrosion Rate x 10^4(mmpy)
Alloy 1	45.1	64.5
Alloy 2	28.3	40.5
Alloy 3	32.5	46.5
Alloy 4	41.1	58.8

Two different discharge current densities were applied 20 mA/cm^2 and 40 mA/cm^2, and the discharge time was 1 hour. Anodic utilization was calculated using Eqs. 2 and 3; also energy density was calculated from Eq. 4.

$$\text{Weight loss}_{\text{theoretical}} = \frac{M\ I\ t}{n\ F} \tag{2}$$

where M is molecular weight of aluminum (g), I is current (A), t is discharge time (s), n is valence electron, F is Faradays constant (96500 Coulombs/gr equivalent)

$$\text{Anode Utilization}(\%) = \frac{\text{Weigth loss}_{\text{therotical}}}{\text{Weight loss}_{\text{experimental}}} x100 \tag{3}$$

Weigth $\text{loss}_{\text{therotical}}$ was calculated from Eq. 2 and Weigth $\text{loss}_{\text{experimental}}$ was obtained using weight of specimen before and after discharge test.

$$\textit{Energy Density} = \frac{E_{operating}\ \ I\ \ t}{\text{Weight loss}_{\text{experimental}}} \tag{4}$$

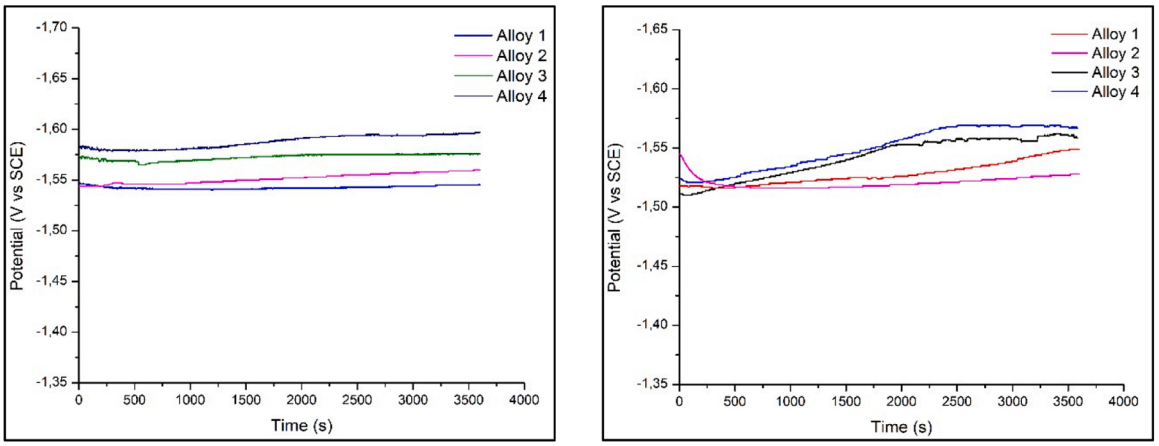

Fig. 5. Discharge behavior of Al-air Alloy 1, Alloy 2, Alloy 3 and Alloy 4 anodes at (a) 20 mA/cm^2, (b) 40 mA/cm^2 for 1 hours in 4 M NaOH.

where $E_{operating}$ is cell potential during discharge test, I is current (A), t is discharge time (s).

3. Results and discussion

Fig. 2 presents SEM images and corresponding EDS results for different alloy compositions after casting process. The second phases were captured using backscatter mode of SEM. All alloys display white phases, and the quantities of these phases increase with Sn content. The percentage of the second-phase area was calculated using ImageJ software, showing ratios of 0.512 %, 0.579 %, 0.660 %, and 0.705 %, respectively, for various alloys. EDS analysis was conducted on the second phases (white regions) at three different points minimum and one result for each alloy is shown in Fig. 2 (C, O and Cl peaks were disabled). As seen, Alloy 1 does not contain Sn in its second phases. The white phases in Alloy 1 are Fe-rich phases, originating from the aluminum. As the Sn content was increased, the second phases consist primarily of Sn, while the amount of Fe-rich precipitates decreases. This may be attributed to the increased Sn content improving the solubility of Fe and Si.

Fig. 3 shows the elemental distribution in aluminum alloy through mapping. Similar to Fig. 2, tin remains in the structure as an undissolved phase. Moreover, the quantity of this secondary phase increases with higher tin content in the alloy, a trend that is clearly given in the mapping. The analysis further indicates that, in addition to tin, iron and silicon contribute to the formation of secondary phases, whereas magnesium exhibits a homogeneous distribution for both alloys.

XRD analysis results are given in Fig. 4, the peak intensities were normalized according to (111) peak for each aluminum alloy. For all the alloys studied, as the amount of tin increases, the peaks shift slightly to the left. The leftward shift of the peaks with increasing tin content indicates lattice expansion. This occurs because tin atoms have a larger atomic radius compared to aluminum atoms. The incorporation of tin atoms into the aluminum lattice structure or the formation of a solid solution leads to an increase in the lattice parameter according to Bragg's law. Additionally, the increase in Sn content within the alloy leads to an increase in the intensity of the (211) peak. This could be attributed to the Sn added to aluminum forming a secondary phase, which indicates the modification of grain orieantation [24].

3.1. Self corrosion

The results of the immersion test are shown in Table 2. The lowest corrosion rate was observed for Alloy 2, which can be explained by two distinct mechanisms involving tin (Sn) in the aluminum alloy. First, Sn possesses a high hydrogen overpotential, which effectively reduces the overall corrosion rate of the aluminum alloy. This elevated overpotential slows down the anodic reaction associated with hydrogen evolution, thereby mitigating corrosion. The hydrogen overpotential of Sn acts as a barrier reducing the rate of the reaction between the aluminum and the alkaline electrolyte, thus lowering the material degradation over time. Second, the solubility of Sn in aluminum is exceptionally low, with a maximum solubility limit of approximately 0.12 wt% [29]. This low solubility promotes the formation of Sn-rich precipitates when the Sn concentration exceeds the solubility threshold. These Sn precipitates can function as cathodic sites within the aluminum matrix, increasing localized galvanic corrosion. The presence of these cathodic centers accelerates the reduction of hydrogen ions, leading to an overall increase in the corrosion rate when the Sn content exceeds the solubility limit. Alloy 2, containing 0.1 wt% Sn, demonstrates an optimized balance between these two mechanisms. The Sn content is within the solubility limit, preventing the formation of significant amounts of Sn precipitates, while the high hydrogen overpotential of Sn helps to reduce the overall corrosion rate. This balance results in a corrosion rate for Alloy 2 that is approximately 40 % lower than that of Alloy 1, which contains no Sn. The absence of Sn in Alloy 1 leaves the alloy vulnerable to faster corrosion, as it lacks the benefits provided by the hydrogen overpotential of Sn. In contrast, Alloy 4, which contains a higher concentration of Sn (above the solubility limit), exhibits a corrosion behavior similar to Alloy 1, despite the presence of Sn. This suggests that in Alloy 4, the precipitate effect becomes the dominant factor, leading to a higher corrosion rate. The excessive Sn precipitates serve as cathodic sites, promoting localized corrosion and negating the beneficial effect of hydrogen overpotential of Sn. The results indicate that a moderate Sn addition (0.1 wt%) can significantly enhance the corrosion resistance of aluminum alloys by reducing the corrosion rate. However, excessive Sn content leads to the formation of cathodic Sn precipitates, which increase corrosion. Therefore, controlling the Sn content within the solubility limit is critical to achieving optimal corrosion resistance in aluminum alloys.

3.1.1. Battery performance

Fig. 5 presents the results of a single-cell test of Al-air batteries with varying aluminum alloy compositions. 20 mA/cm^2 and 40 mA/cm^2 were applied for 1 hour in 4 M NaOH solution. All specimens exhibited similar discharge behavior: the discharge voltage initially dropped, gradually increased over time, and eventually stabilized. This characteristic discharge profile is typical of Al-air batteries, where the initial voltage drop is commonly attributed to the internal resistance of the cell [30]. As the battery discharges, resistance within the electrolyte and the

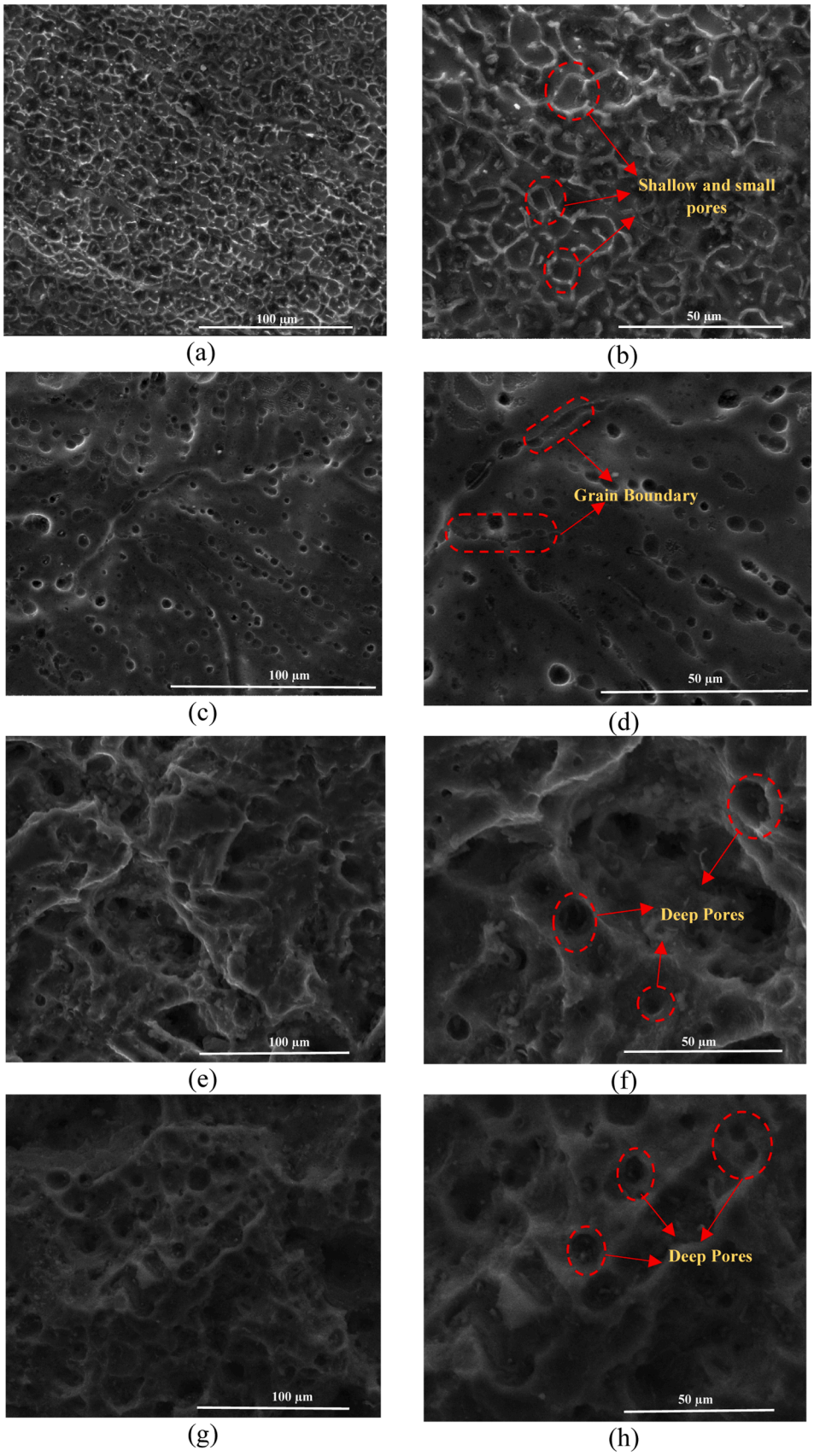

Fig. 6. SEM micrographs of (a), (b) Alloy 1; (c), (d) Alloy 2; (e), (f) Alloy 3 and (g), (h) Alloy 4 subjected to discharge test for 1 h at 40 mA/cm^2 in 4 M NaOH.

Table 3
Calculated discharge test results of Alloy 1, Alloy 2, Alloy 3 and Alloy 4 in 4 M NaOH at 20 mA/cm^2 and 40 mA/cm^2.

Discharge Current Density (mA/cm^2)	Alloy	Energy Density (Wh/kg)	Anode Utilization (%)
20 mA/cm^2	Alloy 1	899	19.6
	Alloy 2	1549	33.3
	Alloy 3	1428	30.4
	Alloy 4	975	20.4
40 mA/cm^2	Alloy 1	1117	30.2
	Alloy 2	1879	50.1
	Alloy 3	1727	45.9
	Alloy 4	1262	33.6

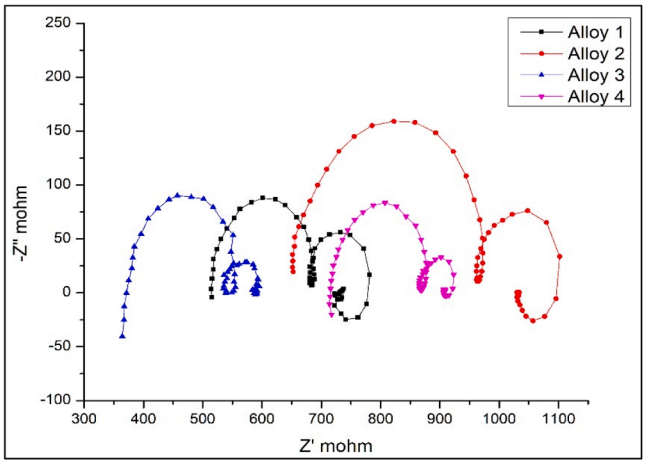

Fig. 7. Nyquist plots of Alloy 1, Alloy 2, Alloy 3 and Alloy 4 in 4 M NaOH.

interfaces between the electrolyte, aluminum anode, and air cathode causes a transient drop in voltage, which stabilizes once the system reaches a steady-state operation. Alloy 4 exhibited the highest operating voltage throughout the test, which can be related to its higher Sn content. Results show that there is a direct correlation between the Sn concentration in the aluminum alloy and the discharge voltage. This relationship can be explained by the ability of Sn to "activate" the aluminum surface, thereby enhancing the electrochemical performance of battery. The presence of Sn, alongside other low-melting-point alloying elements like Ga and In, plays a crucial role in facilitating the reactivity of aluminum anode. These alloying elements, known for their high hydrogen evolution overpotential, participate in a dynamic process of dissolution and redeposition during discharge [15]. Further contributes to improve the discharge voltage through two additional mechanisms. First, Sn forms eutectic mixtures with gallium (Ga) and magnesium (Mg), elements that are present in the alloy. The formation of these eutectics weakens the oxide layer on the surface of the aluminum anode, which is a key factor in enhancing the overall reactivity of the aluminum. By disrupting the oxide film, the Sn-Ga-Mg eutectic mixture allows for more efficient aluminum dissolution during the discharge process, resulting in higher discharge voltages [31]. Second, the Sn-rich phases within the aluminum matrix forms localized galvanic couples between Sn and Al. These findings highlight the importance of alloy composition in optimizing the performance of Al-air batteries, particularly with respect to discharge voltage. For all alloys, the voltage values obtained during discharge tests conducted at high current densities are more fluctuating compared to those at low current densities. This is due to the increased formation of discharge products ($Al(OH)_3$) at high current densities, which hinder ion exchange on the alloy surface. As the tin content increases, the voltage fluctuations also increases. This is attributed to the secondary phases formed by tin, which lead to less uniform dissolution. When a high discharge current density is applied, similar to the low current density tests, the highest discharge voltage is observed for Alloy 3 and Alloy 4. However, their initial voltage is lower compared to the other alloys and increases rapidly over time. During the initial stage of the discharge test, discharge products form rapidly due to the high current density. Over time, the removal of accumulated oxide or hydroxide layers from the initial stage may improve ionic conductivity at the electrode-electrolyte interface, thereby enhancing reaction kinetics.

As shown in Fig. 6, the most homogeneous dissolution was observed in Alloy 1, which contains no tin. Shallow and relatively small pits, uniformly distributed across the surface, were detected (Fig. 6.a.). In contrast, as seen in Fig. 6.b, the corrosion in Alloy 2 is concentrated along the grain boundaries, resulting in less homogeneous dissolution compared to Alloy 1. Fig. 6.c and Fig. 6.d have the formation of deeper pits, likely caused by the inclusion of tin and its associated secondary phases [24].

All samples were weighed before and after the test, and the anodic

Table 4
EIS parameters of different aluminum alloys in 4 M NaOH.

Component	Alloy 1	Alloy 2	Alloy 3	Alloy 4
R_s (Ω)	0.519	0.651	0.375	0.717
R_t (Ω)	0.139	0.200	0.189	0.167
CPE1	$210x10^{-3}$	$296x10^{-3}$	$406x10^{-6}$	$457x10^{-6}$
R_1	0.072	0.089	0.099	0.167
L_1	4.47×10^{-3}	9.08×10^{-3}	689×10^{-6}	791×10^{-6}
R_c	176.9×10^{-3}	357.4×10^{-3}	59.75×10^{-3}	51.95×10^{-3}
CPE2	261×10^{-6}	222×10^{-6}	334×10^{-3}	341×10^{-3}
R_2	1.784	2.904	1.655	1.941
L_2	546×10^{-6}	611×10^{-9}	70×10^{-12}	15.75×10^{-6}

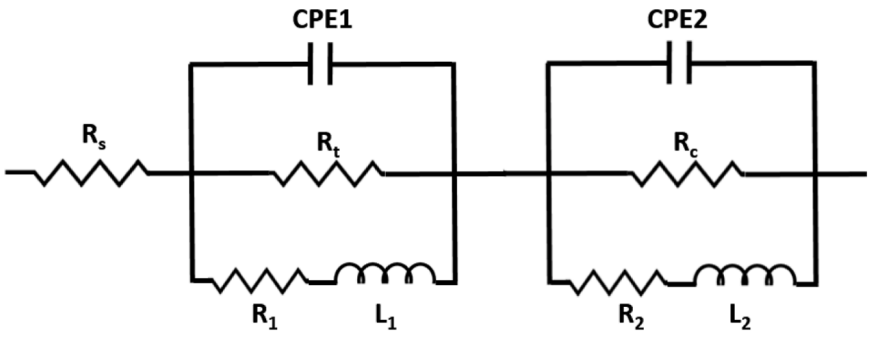

Fig. 8. Equivalent circuit used for fitting the EIS experimental samples.

utilization and energy density were calculated using weight loss based on Eq. 3 and Eq. 4, respectively. The calculated results are listed in Table 3. Higher energy density was obtained at higher discharge current density for all alloys investigated. It may be related to the anodic reaction which becomes the dominant process at high current densities, with less time for competing parasitic reactions (e.g., hydrogen evolution) to occur. The highest energy density and anodic utilization was observed for Alloy 2. The lowest energy density was calculated for Alloy 1 and it is similar to Alloy 4. The discharge test result show that the self-corrosion rate has a direct impact on both energy density and anodic utilization, as self-corrosion causes the anode to be consumed not only for generation of electricity but also by below side reaction related to corrosion:

$$Al + 3\ H_2O \rightarrow Al(OH)_3 + 3/2H_2$$

3.1.2. Electrochemical impedance spectra

Fig. 7 shows Nyquist plots for four different alloy compositions. Each plot consists of two capacitive loops and two inductive circles. The equivalent circuit is shown in Fig. 8. One of the capacitive loops occurs at high frequency (R_t and CPE1), representing the metal dissolution reaction and the electric double layer. The other capacitive loop appears at low frequency (R_c and CPE2), indicating the thickening of the film or barriers on the electrode surface [29,32,33]. The intermediate frequency inductive loop (R_1 and L_1) is associated with the hydrogen evolution reaction, while the low-frequency inductive loop (R_2 and L_2) may result from intergranular corrosion. R_s represents the solution resistance, CPE1 is the electric double layer, R_t is the charge transfer resistance at the aluminum interface, R_c is the diffusion resistance, CPE2 is the dielectric strength of the film, R_2 is the electrical resistance due to the formation of an ionic conduction path through the pores of surface film, and L_2 is the inductance caused by the adsorption of OH- ions [29].

The vales that were obtained from curve fitting are given in Table 4. A higher R_t indicates a lower corrosion rate. Starting with the lowest corrosion rate [29], the order of R_t is Alloy 2 > Alloy 3 > Alloy 4 > Alloy 1. This order confirms the self corrosion test results. R_t increases when Sn content increases and becomes 0.2 Ω for Alloy 2. It is similar for 0.1 wt% and 0.2 wt%. But when the amount of Sn increases to 0.4 wt%, R_t decreases to 0.167 Ω. It may be related to increasing the amount of Sn-rich secondary phases.

4. Conclusion

Aluminum-air batteries (AAB) offer a compelling alternative to lithium-ion batteries due to high energy density, cost-effectiveness, and eco-friendliness. However, challenges such as oxide layer formation and unwanted corrosion reactions on aluminum anodes hinder their efficiency. This research explores the impact of tin (Sn) alloying on the corrosion behavior and discharge performance of aluminum alloys for AABs. Three different Sn concentrations were added into an Al-0.5Mg-0.05Ga-0.05In base alloy, and their performance was assessed using immersion and electrochemical tests in 4 M NaOH solution. The results show that the addition of Sn reduces corrosion rates and enhances discharge efficiency. Addition of 0.1 wt% Sn optimizes the performance in terms of both corrosion resistance and energy density.

CRediT authorship contribution statement

İshak Karakaya: Supervision. **Metehan Erdoğan:** Supervision. **Bilgehan Çetinöz Öksüz:** Writing – original draft.

Declaration of Competing Interest

The authors declare that they have no known competing financial interests or personal relationships that could have appeared to influence the work reported in this paper.

Acknowledgements

The authors would like to thank Middle East Technical University for support on this study.

References

[1] E. De Cian, I. Sue, Global energy consumption in a warming climate, Environ. Resour. Econ. 72 (2019) 365–410, https://doi.org/10.1007/s10640-017-0198-4.
[2] B. Dunn, B. Dunn, H. Kamath, J. Tarascon, For the grid: a battery of choices, Nat. Mater. 928 (2012) 2011–2012, https://doi.org/10.1126/science.1212741.
[3] Y. Li, J. Lu, Metal-air batteries: will they be the future electrochemical energy storage device of choice? ACS Energy Lett. 2 (2017) 1370–1377, https://doi.org/10.1021/acsenergylett.7b00119.
[4] J. Ryu, M. Park, J. Cho, Advanced TEchnologies for High-energy Aluminum–air Batteries, Adv. Mater. 31 (2018) 1804784, https://doi.org/10.1002/adma.201804784.
[5] Z.A. Zafar, S. Imtiaz, R. Razaq, T. Huang, Cathode materials for rechargeable aluminum batteries: current status, J. Mater. Chem. A 5 (2017) 5646–5660, https://doi.org/10.1039/C7TA00282C.
[6] W. Wang, et al., Constructing dilute Mg-1. 0In binary alloy: a pathway to enhanced anode performance in Mg-air battery, J. Power Sources 624 (2024) 235579, https://doi.org/10.1016/j.jpowsour.2024.235579.
[7] J. Liu, et al., Tailoring the microstructure of Mg-Al-Sn-RE alloy via friction stir processing and the impact on its electrochemical discharge behaviour as the anode for Mg-air battery, J. Magnes. Alloy. 12 (2024), https://doi.org/10.1016/j.jma.2022.07.016.
[8] W. Wang, et al., Micro-alloyed Mg – Al – Sn anode with refined dendrites used for Mg-air battery, J. Power Sources 583 (2023) 233569, https://doi.org/10.1016/j.jpowsour.2023.233569.
[9] G.M. Wu, S.J. Lin, C.C. Yang, Alkaline Zn-air and Al-air cells based on novel solid PVA / PAA polymer electrolyte membranes, J. Power Sources 280 (2006) 802–808, https://doi.org/10.1016/j.memsci.2006.02.037.
[10] M.A. Amin, S.S.A. El-rehim, E.E.F. El-sherbini, S.R. Mahmoud, M.N. Abbas, Pitting corrosion studies on Al and Al–Zn alloys in SCN− solutions, Electrochim. Acta 54 (2009) 4288–4296, https://doi.org/10.1016/j.electacta.2009.02.076.
[11] J. Radoˇ, Cathodic Breakdown of Anodic Oxide Film on Al and Al–Sn Alloys in NaCl Solution, Electrochim. Acta 50 (2005) 5624–5632, https://doi.org/10.1016/j.electacta.2005.02.076.
[12] E. Khamis, S. Adeel, Inhibition of aluminum corrosion in alkaline solutions using natural compounds, J. Power Sources 109 (2008) 297–305, https://doi.org/10.1016/j.matchemphys.2007.11.038.
[13] J. Liu, D. Wang, D. Zhang, L. Gao, T. Lin, Synergistic effects of carboxymethyl cellulose and ZnO as alkaline electrolyte additives for aluminium anodes with a view towards Al-air batteries, J. Power Sources 335 (2016) 1–11, https://doi.org/10.1016/j.jpowsour.2016.09.060.
[14] K. Xhanari, Organic Corrosion Inhibitors for Aluminum and Its Alloys in Chloride and Alkaline Solutions: A Review, Arab. J. Chem. 12 (2019) 4646–4663, https://doi.org/10.1016/j.arabjc.2016.08.009.
[15] J. Ma, J. Wen, J. Gao, Q. Li, Performance of Al-0.5 Mg-0.02 Ga-0.1 Sn-0.5 Mn as anode for Al-air battery in NaCl solutions, J. Power Sources 253 (2014) 419–423, https://doi.org/10.1016/j.electacta.2014.02.015.
[16] J. Ma, J. Wen, J. Gao, Q. Li, Performance of Al-1Mg-1Zn-0.1Ga-0.1Sn as anode for Al-air battery, Electrochim. Acta 129 (2014) 69–75, https://doi.org/10.1016/j.electacta.2014.02.080.
[17] Z. Wu, H. Zhang, K. Qin, J. Zou, K. Qin, C. Ban, The role of gallium and indium in improving the electrochemical characteristics of Al – Mg – Sn-based alloy for Al – air battery anodes in 2 M NaCl solution, J. Mater. Sci. 55 (2020) 11545–11560, https://doi.org/10.1007/s10853-020-04755-8.
[18] R. Zhao, P. He, F. Yu, J. Yang, Z. Sun, W. Hu, Performance improvement for aluminum-air battery by using alloying anodes prepared from commercially pure aluminum, J. Energy Storage 73 (2023) 108985, https://doi.org/10.1016/j.est.2023.108985.
[19] W. Ren, W. Ma, S. Zhang, B. Tang, Recent advances in shuttle effect inhibition for lithium sulfur batteries, Energy Storage Mater. 23 (2019) 707–732, https://doi.org/10.1016/j.ensm.2019.02.013.
[20] S. Wei, Y. Xu, S. Tian, Z. Han, L. Xu, Effect of microwave field on microstructure and battery performance of Al-Mg-Sn-Ga anode material, Electrochim. Acta 433 (2022) 2–9, https://doi.org/10.1016/j.electacta.2022.141208.
[21] J. Gao, H. Fan, E. Wang, Y. Song, G. Sun, Exploring the effect of magnesium content on the electrochemical performance of aluminum anodes in alkaline batteries, Electrochim. Acta 353 (2020) 136497, https://doi.org/10.1016/j.electacta.2020.136497.
[22] E. Ghali, in: R. Winston Revie (Ed.), Corrosion Resistance of Aluminum and Magnesium Alloys: Understanding, Performance, and Testing, John Wiley & Sons, Inc, Hoboken, New Jersey, 2010, pp. 121–175.
[23] V.A. Online, J. Arjomandi, Enhanced electrochemical performance of Al-0.9Mg-1Zn-0.1Mn-0.05Bi-0.02In fabricated from commercially pure aluminum for use as anode of alkaline batteries, RSC Adv. 6 (2016) 28055–28062, https://doi.org/10.1039/C6RA02113A.
[24] H. Xiong, Z. Wang, H. Yu, T. Chen, X. Wang, L. Ye, Performances of Al-xLi alloy anodes for Al-air batteries in alkaline electrolyte, J. Alloy. Compd.. 889 (2021) 161677, https://doi.org/10.1016/j.jallcom.2021.161677.

[25] D.D. Macdonald, K.H. Lee, A. Moccari, D. Harrington, Evaluation of alloy anodes for aluminum-air batteries: corrosion studies, J. Electrochem. Sci. 1 (1988) 652–657, https://doi.org/10.5006/1.3584979.
[26] X. Xu, J. Zhang, Y. Deng, Discharge performance of the Al–Mg–Sn alloy anodes with different Sn content for Al-air batteries, J. Power Sources 576 (2023) 233236, https://doi.org/10.1016/j.jpowsour.2023.233236.
[27] M. Elrouby, M. Abdelsamie, Effect of Sn and Zn alloying with Al on its electrochemical performance in alkaline media containing CO2 for Al-air batteries application, Int. J. Hydrog. Energy 48 (2023) 27960–27977, https://doi.org/10.1016/j.ijhydene.2023.03.469.
[28] M. Quan, Y. Sui, Y. Jiang, The influence of Sn content on the electrochemical performance and discharge characteristics of Al-0.2Mg-0.02In-xSn-0.02Bi alloy anodes in aluminum-air batteries, Ioics 30 (2024) 3309–3318, https://doi.org/10.1007/s11581-024-05517-1.
[29] C. Zhu, H. Yang, A. Wu, D. Zhang, L. Gao, T. Lin, Modified alkaline electrolyte with 8-hydroxyquinoline and ZnO complex additives to improve Al-air battery, J. Power Sources 432 (2019) 55–64, https://doi.org/10.1016/j.jpowsour.2019.05.077.
[30] M.R. Sovizi, M. Afshari, K. Jafarzadeh, J. Neshati, Electrochemical and microstructural investigations on an As-cast and solution-annealed Al–Mg–Sn–Ga alloy as anode material in sodium chloride solution, J. Power Sources 3073 (2017) 3073–3084, https://doi.org/10.1007/s11581-017-2099-5.
[31] M. Srinivas, S. Kumar, L. Neelakantan, Solubility effects of Sn and Ga on the microstructure and corrosion behavior of Al-Mg-Sn-Ga alloy anodes, J. Alloy. Compd. 683 (2016) 647–653, https://doi.org/10.1016/j.jallcom.2016.05.090.
[32] S. Yin, et al., Improving the corrosion resistance of MgZn1.2GdxZr0.18 (x = 0, 0.8, 1.4, 2.0) alloys via Gd additions, Corros. Sci. 177 (2020) 108962, https://doi.org/10.1016/j.corsci.2020.108962.
[33] Q.X. Kang, T.Y. Zhang, X. Wang, Y. Wang, X.Y. Zhang, Effect of cerium acetate and L-glutamic acid as hybrid electrolyte additives on the performance of Al-air battery, J. Power Sources 443 (2019) 227251, https://doi.org/10.1016/j.jpowsour.2019.227251.